Polymer Chemistry

Functionalization-Induced Self-Assembly Under Ambient Conditions via Thiol-Epoxide "Click" Chemistry

Journal:	*Polymer Chemistry*
Manuscript ID	PY-COM-07-2019-001144.R1
Article Type:	Communication
Date Submitted by the Author:	20-Sep-2019
Complete List of Authors:	Howe, David; Drexel University, Materials Science and Engineering Jenewein, Ken; Fachhochschule Munster - Standort Steinfurt; Drexel University, Materials Science and Engineering Hart, James; Drexel University, Materials Science and Engineering Taheri, Mitra; Drexel University, Materials Science and Engineering Magenau, Andrew; Drexel University, Materials Science and Engineering

Functionalization-Induced Self-Assembly Under Ambient Conditions via Thiol-Epoxide "Click" Chemistry

Received 00th January 20xx,
Accepted 00th January 20xx

DOI: 10.1039/x0xx00000x

David H. Howe, ‡[a] Ken J. Jenewein, ‡[a] James L. Hart,[a] Mitra L. Taheri,[a] and Andrew J. D. Magenau*[a]

Polymer micelles were formed using thiol-epoxide "click" chemistry to trigger functionalization-induced self-assembly (FISA) of block copolymers by modifying a reactive glycidyl methacrylate block with solvophobes. Ambient conditions, polymer concentrations up to 10 wt%, and an array of functional thiols were found effective for nanoparticle synthesis. Real-time analysis enabled direct observation of the self-assembly process, revealing mechanistic details and a critical degree of functionalization required for micellization.

The sophisticated, multiscale organization witnessed in nature has long inspired scientists to develop similar self-assembly processes for synthetic materials.[1-3] Advances in such self-assembly processes have given rise to new nanomaterials with prospective applications in drug delivery,[4, 5] water purification,[6-8] microelectronics,[3, 9, 10] and catalysis.[11-13] Traditionally, the self-assembly of block copolymers (BCPs) in solution has relied upon widely-used solvent-displacement methods, which gradually change the solvent composition through addition of a precipitant to selectively desolvate one block.[1, 14] While successful for attaining a broad array of self-assembled morphologies and compositions, the low solid content hinders scale-up and industrial viability, motivating the development of new processes.[15, 16]

An alternate strategy to self-assembled nanostructures can be accomplished by inducing self-assembly through polymerization, chain-cleavage, or polymer modification. Polymerization-induced self-assembly (PISA) has garnered significant attention because of its efficacy at high solid content (~10-50% w/w), reduced number of reaction steps to final product, and compatibility with numerous polymerization techniques including atom transfer radical polymerization,[17] nitroxide mediated polymerization,[18] organotellurium mediated radical polymerization,[19] ring-opening metathesis polymerization,[20, 21] and reversible addition-fragmentation chain transfer (RAFT) polymerization.[16] During PISA, a soluble homopolymer is chain extended with a monomer and as polymerization progresses, an immiscible block is gradually formed that drives in situ self-assembly. PISA grants access to an assortment of morphologies (spheres, cylinders, vesicles, etc.), primarily through the targeted ratio of solvophilic to solvophobic block lengths which dictate the critical packing parameter.[16, 22, 23] A corollary technique, polymerization induced microphase separation, operates through a similar principle as PISA but with bulk conditions and crosslinker, enabling the fabrication of highly-tunable nanoporous materials for applications in filtration and heterogeneous catalysis.[24, 25] Other mechanisms have been developed to induce self-assembly (or other phase transitions) through grafting-from polymerization,[26] chain-scission of hydrophobic blocks,[27] and deprotection[28] or functionalization of BCPs.[29, 30]

Inspired by these approaches, our group and another introduced a new mechanism for inducing self-assembly through post-polymerization modification (PPM),[29, 30] which we termed functionalization-induced self-assembly (FISA). In our report, we utilized Pd-catalyzed Suzuki–Miyaura cross-coupling as a PPM technique to generate BCP amphiphilicity from an initially soluble BCP.[30, 31] During FISA, the pendant groups of one block are chemically modified by successive installation of solvophobes that steadily increase the BCP's amphiphilicity until phase separation occurs, resulting in micelle formation. One unique aspect of FISA is the isolation of side-chain chemistry as the defining parameter governing self-assembly, as PPM keeps constant the degree of polymerization, tacticity, and dispersity between different BPC products originating from the same BCP precursor.[32, 33] In addition, a vast number of efficient PPM reactions could be adapted to FISA (e.g., activated esterification,[34] Diels-Alder cycloaddition,[35, 36] thiol-ene/thiol-yne addition,[37-39] and azide-alkyne cycloadditions)[40-42] offering immense tailorability to micelle core compositions and structures.

[a] *Department of Materials Science and Engineering, Drexel University College of Engineering, 3141 Chestnut Street, Philadelphia, Pennsylvania, 19104, USA. Email: ajm496@drexel.edu*

† Electronic Supplementary Information (ESI) available. See DOI: 10.1039/x0xx00000x

‡ These authors contributed equally.

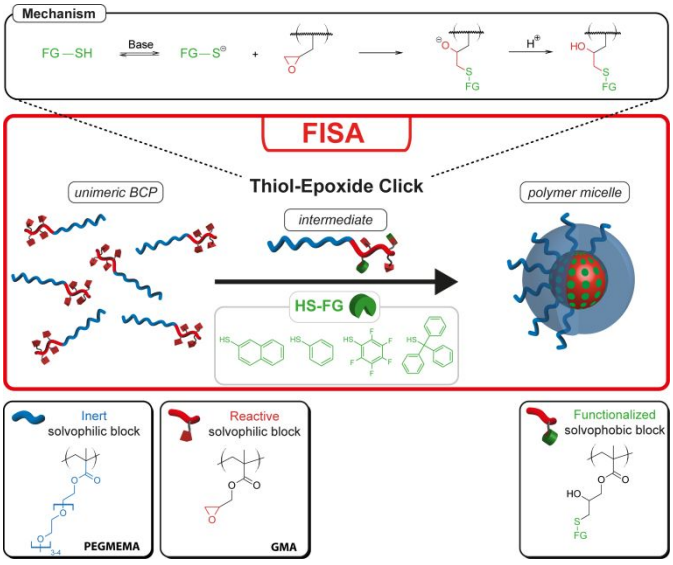

Scheme 1. Polymer micelles from FISA of diblock copolymers using solvophobic functional groups installed with thiol-epoxide "click" chemistry.

Although FISA through cross-coupling was effective for synthesizing tailorable polymer micelles, this system has drawbacks including oxygen sensitivity, heterogeneous reagents, and residual and expensive Pd-catalyst. To address these shortcomings, we report for the first time, a thiol-epoxide "click" based system (Scheme 1). The versatility of epoxides provides a promising avenue to expand FISA since ring-opening is possible with numerous classes of nucleophiles, e.g., amines, azides, and thiols.[43, 44] In particular, base-catalyzed thiol-epoxide reactions are especially attractive because of their 100% atom efficiency, rapid reaction rates, high conversions (> 90%), and efficacy under mild and ambient conditions.[45-47] The thiol-epoxide reaction proceeds by deprotonation of the thiol by a base, thiolate attack on the epoxide's less hindered carbon (S_N2 type) and alkoxide formation, and subsequent proton transfer to generate the final thiol-ether functionalization product (Scheme 1).[44] Furthermore, the vast number of commercially available functional thiols lends itself to customizable micellar cores, which we envision as a pragmatic tool for potentially meeting a variety of application needs, specifically for cargo encapsulation and release, via judicious selection of the functional reaction partner.

We designed our BCP precursor for FISA to be comprised of a glycidyl methacrylate (GMA) reactive block and a poly(ethylene glycol) methyl ether methacrylate (PEGMEMA) inert stabilizer block (Scheme 1). The thiol-epoxide ring-opening reaction is well-established with p(GMA),[43] and p(PEGMEMA) has excellent solubility in both organic and aqueous media.[48] The first p(GMA) block was polymerized using photoinduced electron transfer-RAFT (PET-RAFT), employing eosin Y (EY) as the photocatalyst and 4-cyanopentanoic acid dithiobenzoate as the chain transfer agent (CTA) because phenolic Z-groups are known to be effective with methacrylic monomers.[49, 50] Kinetic analysis of PET-RAFT revealed high monomer conversion (>80 %) after 10 hours and pseudo first-order behaviour indicative of a constant number of propagating species (Figure 1A). As the polymerization progressed, size exclusion chromatography (SEC) showed that the number-average molecular weight (M_n) gradually increased and that the polymer dispersity decreased ($Đ \approx 1.20$ to 1.13) (Figure 1B). Subsequent chain-extension of p(GMA) with PEGMEMA using PET-RAFT resulted in a large increase in M_n with the absence of any significant amount of residual macro-CTA, confirming successful BCP formation and high livingness of our macro-CTA (Figure 1C). The final BCP used for FISA experiments had a M_n = 27.2 kg/mol and a $Đ$ = 1.20, consisting of 35 GMA and 73 PEGMEMA repeat units. Structural confirmation of p(GMA-*b*-PEGMEMA) was made using proton nuclear magnetic resonance (^{1}H-NMR), which showed preservation of the epoxide ring resonances in the GMA block (a, b, and c) and the presence of typical resonances of the PEGMEMA block (d, e, and f, Figure 1D).

Our initial attempt at FISA was performed using 2-naphthalenethiol due to its anticipated likelihood for forming solvophobic adducts in ethanol, leading to micellization after reaction with the p(GMA) block (Table 1). The thiol-epoxide ring-opening reaction was carried out under fully ambient conditions (at room temperature and in air) using a 1.25 molar excess of the thiol and employing potassium hydroxide (KOH) as the base. Initial reaction mixtures were found to be homogenous with BCP precursors having a mean hydrodynamic diameter (D_H) of ~17 nm at 3 wt% (ethanol and BCP only), according to number distributions from dynamic light scattering (DLS) (Figure 2A, Table 1). DLS measurements under true FISA conditions, with base and thiol present, exhibited number-average diameters less than 10

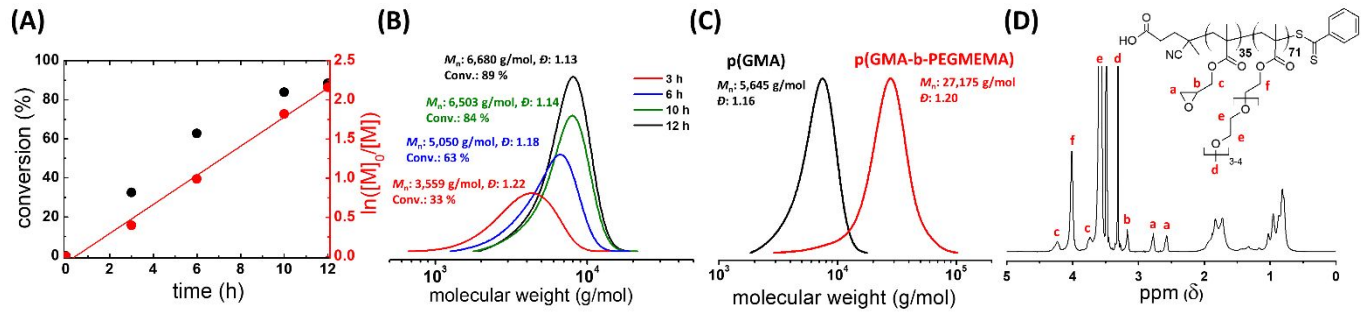

Figure 1. (A) PET-RAFT of GMA in DMSO with a GMA|CTA|EY molar ratio of 40|1|0.004 at 40 wt% monomer for 12 h. Monomer conversion as a function of time and pseudo first-order kinetic plot with a linear fit. (B) Corresponding SEC traces of kinetic samples with M_n, $Đ$, and monomer conversion. (C) Chain extension of p(GMA) with PEGMEMA using a PEGMEMA|Macro-CTA|EY molar ratio of 120|1|0.006 in 20 wt% PEGMEMA for 9.5 h. (D) ^{1}H-NMR spectra of p(GMA-*b*-PEGMEMA) measured in $CDCl_3$.

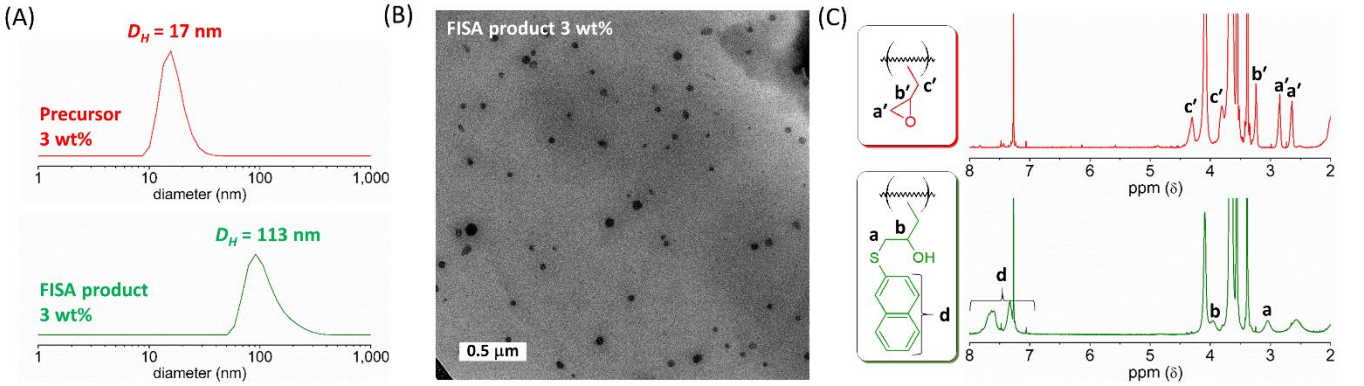

Figure 2. FISA with 2-napthalenethiol under conditions in Table 1 Entry 2. (A) DLS number distributions for unimer precursor (top) at 3 wt% BCP and of the crude reaction product for FISA reaction. (B) TEM micrograph of the crude reaction product after FISA. (C) ^{1}H-NMR spectra of p(GMA-*b*-PEGMEMA) precursor in $CDCl_3$ before functionalization (top) and of the purified product after functionalization (bottom).

nm consistent in size with BCP unimers (see subsequent kinetic study).

FISA was commenced by introduction of base and then allowed to react for 20 hours before DLS and microscopy evaluation of the resulting particles and ^{1}H-NMR analysis to confirm functionalization. Once FISA was complete, the final particle size showed a pronounced increase in size to ~113 nm by DLS (Figure 2A) with a narrow particle size distribution (polydispersity index (PDI) = 0.15)). Notably, the FISA product was evaluated with DLS at the same concentration as the reaction (3 wt% BCP) without any post-processing. Transmission electron microscopy (TEM) in Figure 2B supports the approximate size range reported by DLS and confirms our supposition that spherical polymer nanoparticles should form based upon the relative solvophilic to solvophobic block lengths of our BCP. ^{1}H-NMR spectra of the precursor and final purified product are shown in Figure 2C. The effectiveness of the reaction was verified by nearly complete elimination of the epoxide group resonances (a', b', and c'), yielding a percent functionalization (%*f*) of 90% using an integral from the emergent resonance at 3.04 ppm (a), characteristic of the CH_2 group adjacent to the sulfur atom after ring-opening, or from the newly installed naphthalene pendent groups (d) (see the SI for further details concerning %*f* calculations). It should be noted that while functionalization is effective and stable under FISA conditions (with thiol), prolonged exposure of the BCP precursor to base for 20 h without thiol present resulted in degradation of the epoxide groups. As a last characterization tool and to confirm our self-assembled particles were non-covalent, SEC analysis was performed on the final BCP, which revealed a monomodal and low dispersity product without signs of any covalently crosslinked by-products (Figure S4). Following our initial demonstration of FISA, we sought to demonstrate whether FISA could be carried out at a higher solid content of 10 wt% BCP with 2-napthalenethiol (Table 1, Entry 3). Comparatively, FISA at 10 wt% resulted in self-assembled particles of similar size (~95 nm) and a small fraction of larger structures according to DLS, but also with quantitative %*f* which we attribute to faster reaction rates from higher reactant concentrations (Figure S5).

The reactions described up to this point support the efficacy of the thiol-epoxide reaction as a trigger for FISA, however, significant questions remain in terms of the kinetics and thermodynamics governing this self-assembly process. Toward this goal, we designed a FISA experiment that would allow simultaneous real-time observation of the particle size during FISA overlaid with kinetic monitoring of the functionalization reaction. This real-time FISA experiment was executed directly in a DLS cuvette under conditions summarized in Table 1 Entry 4, with aliquots being withdrawn every ~20 minutes for NMR after addition of the base. Figure 3A shows the real-

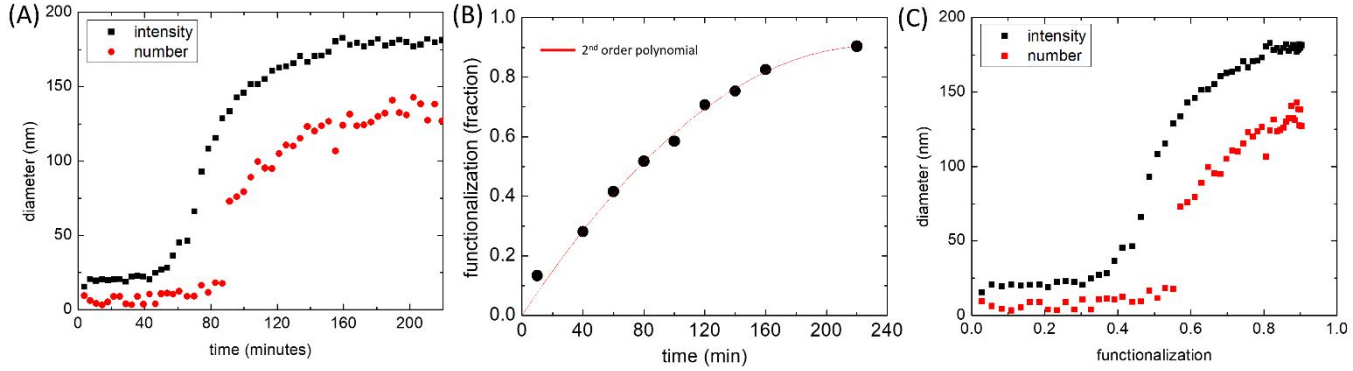

Figure 3. Real-time FISA and in-situ micellization of p(GMA-*b*-PEGMEMA) with 2-naphthalenethiol under conditions in Table 1 Entry 4. (A) Mean hydrodynamic diameter from real-time DLS, calculated from number and intensity distributions. (B) Kinetics of BCP functionalization evaluated by ^{1}H-NMR. (C) Plot of the degree of functionalization versus the hydrodynamic diameter generated by combining data from Figure A and B using a correlation function.

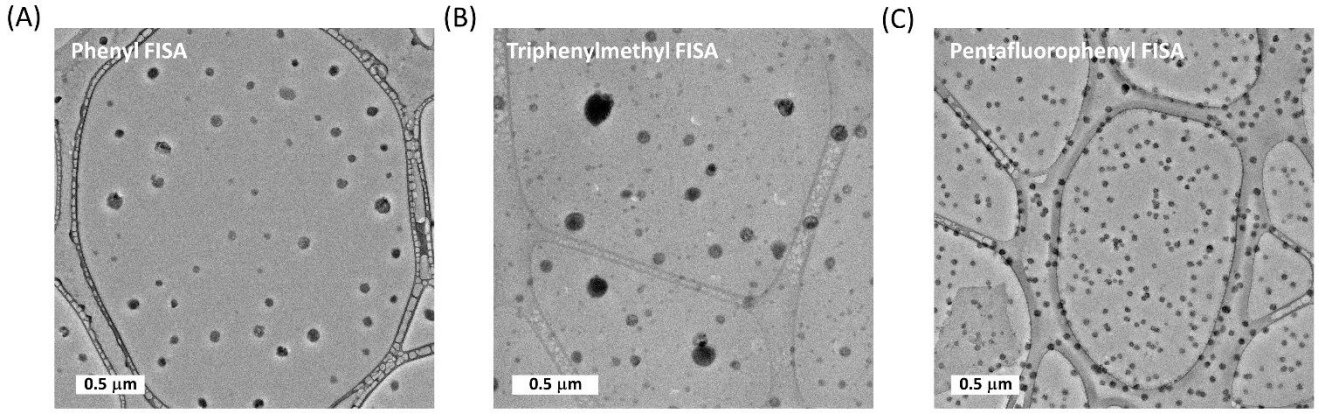

Figure 4. TEM images of crude FISA reaction products prepared from (A) thiophenol functionalization (Table 1, Entry 5), (B) triphenylmethanelthiol functionalization (Table 1, Entry 6), and (C) pentafluorothiophenol functionalization (Table 1, Entry 7).

time DLS result, consisting of the instantaneous mean hydrodynamic diameter of the most prominent peak from DLS intensity and number distributions. Based on the intensity distribution data, we observed four major regions during the FISA processes: (1) an induction region with fairly constant particle size in the range of precursors/unimers, (2) a transition region of rapid growth (and the onset of micellization) traversing into the size range of polymer micelles, (3) a growth region (post self-assembly) characteristic of continued but slower micelle growth, and (4) a final plateau region at the conclusion of FISA. Using Figure 3A, a critical time to self-assembly was extracted from the intensity plot at ~75 min defined at the mid-point diameter of ~100 nm. Similar behaviour was observed in the number distribution data, however the intensity data exhibited less noise and a more gradual onset of self-assembly. Kinetic samples for NMR during FISA helped to paint a more detailed picture of the self-assembly process, elucidating the BCP's composition during each region of FISA. Based on ^{1}H-NMR analysis, %*f* values were calculated at each time point shown in Figure 3B, during the same real-time DLS experiment from Figure 3A. At early reaction times, the reaction rate was found to be rapid reaching ~45 %*f* in the first hour, whereas at later times, the reaction rate became progressively more sluggish requiring 2 additional hours to double (~90%). It should be noted that initial attempts at determining the kinetics of functionalization were unsuccessful as the thiol-epoxide reaction continued even after sampling, yielding close-to quantitative functionalization at all time points (underscoring the robust nature of this reaction). To resolve this issue, a novel quenching procedure was developed by introducing a large excess of electrophile (i.e., 3-bromo-1-propanol) to each NMR sample for competitive consumption of the thiolate nucleophile. This strategy proved successful and was verified by performing parallel reactions with and without quenching agent (see SI and Figure S7 for further details). To shed light on the FISA mechanism, we combined results from Figures 3A and B to produce a new plot depicting the relationship between the degree of functionalization and D_H during the course of FISA (Figure 3C). Through a correlation function between %*f* and time (Figure 3B: red line, R^2 = 0.99), each time point in Figure 3A could be converted into a functionalization value in Figure 3C. This allowed us to uncover several key features of the FISA process: (1) FISA likely proceeds through a partially functionalized intermediate as the average particle size remains unimeric even as functionalization is progressing during early stages of the reaction, (2) a critical %*f* appears to exist to invoke spontaneous self-assembly marked by a rapid change in D_H, i.e., for naphthalenethiol in ethanol this threshold is ~40% functionalization (or ~15 solvophobes) when using the intensity distribution, and (3) functionalization persists even after self-assembly and the micelle size continues to evolve as functionalization progresses. We anticipate this experimental approach will allow for a more nuanced understanding of micellization behaviour and structure-property relationships in FISA (or other self-assembly processes) when expanded in more comprehensive investigations.

In order to demonstrate the versatility of FISA, three additional thiols were tested using thiol-epoxide ring-opening. FISA was employed using identical conditions established for naphthalenethiol but instead with thiophenol, triphenylmethanethiol, and pentafluorothiophenol (Scheme 1). All prior reactions with naphthalenethiol are summarized in Table 1 Entries 2-4. Notably, all three functionalities were found to achieve nearly quantitative conversion (≥ 98%) of the epoxide groups after 20 hours (Table 1 Entries 5-7 and Figures S8-S10). In each case, polymer micelles of a range of sizes were observed in TEM micrographs as shown in Figure 4. DLS measurements also confirmed self-assembly and the presence of polymer micelles and other large structures (see Table 1 and SI for further details). The readily formed nanoparticles from four different functional groups indicate the suitability of thiol-epoxide ring-opening as a convenient and robust reaction for implementing FISA.

Table 1. Summary of FISA reaction conditions and results.

Entry	Functionality	Reaction conditions			NMR results	DLS_{Number}	
		Catalyst Conc. (mol%)	BCP Conc. (wt%)	Time (h)	Functionalization (%)	Mean (nm)	PDI
1	(Precursor)	-	3	-	-	17	0.06
2	Naphthalene	10	3	20	90	113	0.15
3	Naphthalene	10	10	20	>99	95	0.10
4	Naphthalene	2	2.5	3.5	90	127	0.15
5*	Phenyl	10	3	20	>99	158	0.55
6	Triphenylmethane	10	3	20	>99	93	0.19
7**	Pentafluorophenyl	10	3	20	98	44	0.17

* DLS results after a 12-fold dilution of the sample.
** DLS results from a purified and reconstituted sample.

In conclusion, we demonstrated for the first time, a new functionalization reaction for FISA based on thiol-epoxide ring-opening to access various nanostructures from a diblock copolymer. Results have shown that this system can be carried out at room temperature and under ambient conditions to high degrees of functionalization, ultimately triggering micellization. This synthetic approach has been demonstrated to be robust and tolerant to a range of functionalities, as shown by its scalability and utility with four different reaction partners. In addition, real-time observation of FISA was possible with DLS allowing direct monitoring of the in situ self-assembly process and particle size evolution. When coupled with kinetic analysis, reaction rates and the degree of functionalization were ascertained during FISA, demonstrating a promising approach for interrogating the FISA process and gaining new insights into the self-assembly mechanism. Ongoing efforts are focused on establishing a better understanding of how the precursor structure and installed functionality define the self-assembly process, morphology, and properties of FISA-derived structures.

Conflicts of interest

There are no conflicts to declare.

Acknowledgements

This work was supported by the Department of Education's GAANN Fellowship award program (P200A150240). AJDM would like to thank the ACS Petroleum Research Fund (59903-DNI7) for partial support of this research and Drexel University for startup funds. J.L.H. and M.L.T. acknowledge funding from the National Science Foundation Major Research Instrumentation award (DMR-1429661). The authors thank Kathleen Maleski and Dr. Yury Gogotsi for instrument access and advice regarding DLS, Sam J. Rozans and Olivia R. Wilson for helpful experimental discussions, and MarvinSketch for generous allowance of an academic license.

Notes and references

1 Y. Mai; A. Eisenberg, *Chem. Soc. Rev.*, 2012, **41**, 5969.
2 I. W. Hamley, *Angew. Chem. Int. Ed.*, 2003, **42**, 1692.
3 G. M. Whitesides; B. Grzybowski, *Science*, 2002, **295**, 2418.
4 C. J. Drummond; C. Fong, *Curr. Opin. Colloid Interface Sci.*, 1999, **4**, 449.
5 H. Cabral; K. Miyata; K. Osada; K. Kataoka, *Chem. Rev.*, 2018, **118**, 6844.
6 L.-S. Zhong; J.-S. Hu; H.-P. Liang; A.-M. Cao; W.-G. Song; L.-J. Wan, *Adv. Mater.*, 2006, **18**, 2426.
7 Q. Fang; B. Chen, *J. Mater. Chem. A*, 2014, **2**, 8941.
8 W. A. Phillip; B. O'Neill; M. Rodwogin; M. A. Hillmyer; E. L. Cussler, *ACS Appl. Mater. Interfaces*, 2010, **2**, 847.
9 G. Whitesides; J. Mathias; C. Seto, *Science*, 1991, **254**, 1312.
10 H.-C. Kim; S.-M. Park; W. D. Hinsberg, *Chem. Rev.*, 2010, **110**, 146.
11 I. P. Beletskaya; A. N. Kashin; A. E. Litvinov; V. S. Tyurin; P. M. Valetsky; G. van Koten, *Organometallics*, 2006, **25**, 154.
12 S. Sugihara; M. Sudo; Y. Maeda, *Langmuir*, 2019, **35**, 1346.
13 J. Lü; Y. Yang; J. Gao; H. Duan; C. Lü, *Langmuir*, 2018, **34**, 8205.
14 L. Zhang; A. Eisenberg, *Science*, 1995, **268**, 1728.
15 U. Tritschler; S. Pearce; J. Gwyther; G. R. Whittell; I. Manners, *Macromolecules*, 2017, **50**, 3439.
16 S. L. Canning; G. N. Smith; S. P. Armes, *Macromolecules*, 2016, **49**, 1985.
17 G. Wang; M. Schmitt; Z. Wang; B. Lee; X. Pan; L. Fu; J. Yan; S. Li; G. Xie; M. R. Bockstaller; K. Matyjaszewski, *Macromolecules*, 2016, **49**, 8605.
18 G. Delaittre; J. Nicolas; C. Lefay; M. Save; B. Charleux, *Soft Matter*, 2006, **2**, 223.
19 M. Okubo; Y. Sugihara; Y. Kitayama; Y. Kagawa; H. Minami, *Macromolecules*, 2009, **42**, 1979.
20 D. B. Wright; M. A. Touve; L. Adamiak; N. C. Gianneschi, *ACS Macro Lett.*, 2017, **6**, 925.
21 D. B. Wright; M. A. Touve; M. P. Thompson; N. C. Gianneschi, *ACS Macro Lett.*, 2018, **7**, 401.
22 M. J. Derry; L. A. Fielding; S. P. Armes, *Prog. Polym. Sci.*, 2016, **52**, 1.
23 N. J. Warren; S. P. Armes, *J. Am. Chem. Soc.*, 2014, **136**, 10174.
24 J. Park; K. Kim; M. Seo, *Chem. Commun.*, 2018, **54**, 7908.
25 M. Seo; M. A. Hillmyer, *Science*, 2012, **336**, 1422.
26 E. S. Zofchak; J. A. LaNasa; W. Mei; R. J. Hickey, *ACS Macro Lett.*, 2018, **7**, 822.
27 B. H. Jones; G. D. Bachand; S. H. R. Shin; M. A. Firestone; W. F. Paxton, *Macromolecules*, 2018, **51**, 6543.
28 X. Wu; L. Su; G. Chen; M. Jiang, *Macromolecules*, 2015, **48**, 3705.
29 S. Li; J. Wang; J. Shen; B. Wu; Y. He, *ACS Macro Lett.*, 2018, **7**, 437.
30 D. H. Howe; J. L. Hart; R. M. McDaniel; M. L. Taheri; A. J. D. Magenau, *ACS Macro Lett.*, 2018, **7**, 1503.
31 D. H. Howe; R. M. McDaniel; A. J. D. Magenau, *Macromolecules*, 2017, **50**, 8010.
32 E. Blasco; M. B. Sims; A. S. Goldmann; B. S. Sumerlin; C. Barner-Kowollik, *Macromolecules*, 2017, **50**, 5215.
33 K. A. Günay; P. Theato; H.-A. Klok, *J. Polym. Sci., Part A: Polym. Chem.*, 2013, **51**, 1.
34 A. Das; P. Theato, *Chem. Rev.*, 2016, **116**, 1434.
35 G. Delaittre; N. K. Guimard; C. Barner-Kowollik, *Acc. Chem. Res.*, 2015, **48**, 1296.
36 M. A. Tasdelen, *Polym. Chem.*, 2011, **2**, 2133.
37 A. J. D. Magenau; J. W. Chan; C. E. Hoyle; R. F. Storey, *Polym. Chem.*, 2010, **1**, 831.
38 A. J. D. Magenau; T. R. Hartlage; R. F. Storey, *J. Polym. Sci., Part A: Polym. Chem.*, 2010, **48**, 5505.
39 C. E. Hoyle; A. B. Lowe; C. N. Bowman, *Chem. Soc. Rev.*, 2010, **39**, 1355.
40 H. C. Kolb; M. G. Finn; K. B. Sharpless, *Angew. Chem. Int. Ed.*, 2001, **40**, 2004.
41 K. Kempe; A. Krieg; C. R. Becer; U. S. Schubert, *Chem. Soc. Rev.*, 2012, **41**, 176.
42 Y. Shi; X. Cao; H. Gao, *Nanoscale*, 2016, **8**, 4864.
43 E. Muzammil; A. Khan; M. C. Stuparu, *RSC Adv.*, 2017, **7**, 55874.
44 M. C. Stuparu; A. Khan, *J. Polym. Sci., Part A: Polym. Chem.*, 2016, **54**, 3057.
45 C.-J. Li; B. M. Trost, *PNAS*, 2008, **105**, 13197.
46 I. Gadwal; A. Khan, *RSC Adv.*, 2015, **5**, 43961.
47 I. Gadwal; J. Rao; J. Baettig; A. Khan, *Macromolecules*, 2014, **47**, 35.
48 A. J. D. Magenau; S. Saurabh; S. K. Andreko; C. A. Telmer; B. F. Schmidt; A. S. Waggoner; M. P. Bruchez, *Biomaterials*, 2015, **66**, 1.
49 S. Perrier, *Macromolecules*, 2017, **50**, 7433.

50 M. Benaglia; E. Rizzardo; A. Alberti; M. Guerra, *Macromolecules*, 2005, **38**, 3129.

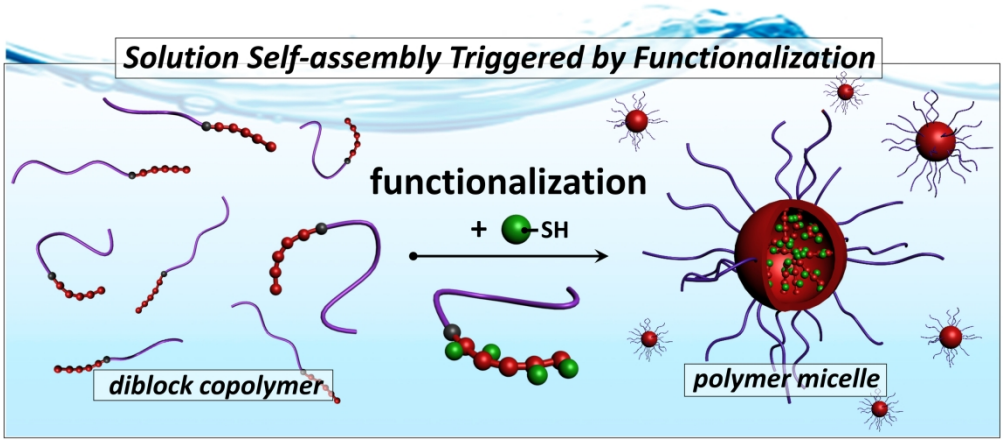

248x110mm (300 x 300 DPI)